

The Effect of Germanium Fraction on High-Field Band-to-Band Tunneling in p^+ -SiGe/ n^+ -SiGe Junctions in Forward and Reverse Biases

Jiun-Yun Li, *Student Member, IEEE*, and James C. Sturm, *Fellow, IEEE*

Abstract—The dependence of band-to-band tunneling in p^+ -Si_{1-x}Ge_x/ n^+ -Si_{1-x}Ge_x homojunctions on Ge fraction and electric field is investigated in the range $2\text{--}3 \times 10^8$ V/m. Negative differential resistance (NDR) in forward bias is observed for each device with the highest peak tunneling-current density of 8.2 kA/cm^2 without any postannealing step. Reverse-biased band-to-band tunneling, as relevant for tunneling field-effect transistors, is also measured. Tunneling via junction defects can mask band-to-band tunneling and the observation of NDR at forward bias confirms negligible tunneling via those defects. Both forward-biased and reverse-biased data are compared with models versus electric field and Ge fraction.

Index Terms—Band-to-band tunneling (BTBT), chemical vapor deposition (CVD), negative differential resistance (NDR), SiGe, tunnel diode, tunneling field-effect transistor (TFET).

I. INTRODUCTION

BAND-TO-BAND tunneling field-effect transistors (TFETs) are promising for ultralow power applications because the operation of low supply voltage can be enabled by their steep subthreshold slopes [1]. While silicon TFETs with subthreshold slopes < 60 mV/decade have been demonstrated, the drive current is low because of the low band-to-band tunneling probability of electrons due to the large bandgap energy of silicon [2]. High drive current can be achieved by replacing silicon with Si_{1-x}Ge_x alloys because of the smaller bandgap energy in Si_{1-x}Ge_x alloys [3]. In addition, a steeper subthreshold slope was suggested by increasing the germanium fraction in a SiGe TFET [4].

To improve the performance of the SiGe TFETs, a careful calibration of SiGe band-to-band tunneling (BTBT) such as the effects of Ge fraction and doping concentrations is required. Previous papers on tunneling in SiGe/Si heterojunctions have not related the BTBT to the electric field [5], [6] or addressed the role of junction defects on BTBT [7]. Furthermore, there is no report on tunneling in the SiGe/SiGe homojunctions.

In this paper, we study BTBT at forward bias and reverse bias in epitaxially grown p^+ -SiGe/ n^+ -SiGe tunneling diodes

by varying the Ge fraction and boron concentration. Negative differential resistance (NDR) at small forward bias, a critical indication of BTBT [8] is observed for each device. A peak tunneling-current density of 8.2 kA/cm^2 at room temperature is also reported, the highest among all Si-based tunneling diodes grown by chemical vapor deposition (CVD) so far. We also discuss the effects of junction defects on the tunneling current and use NDR at forward bias to confirm that the observed current is dominated by BTBT rather than defect-assisted tunneling (DAT) [9]. The sets of experimental data at forward and reverse biases are compared with models versus Ge fraction and electric field to serve as a baseline calibration for device modeling programs.

In this paper, we first introduce the epitaxial growth and fabrication of SiGe-based tunneling diodes in Section II. Then we discuss BTBT at forward bias with a model comparison in Section III. In Section IV, we discuss the reverse-biased data and modeling, followed by a brief conclusion in Section V.

II. EXPERIMENT

The device structure of the experimental p^+ -SiGe/ n^+ -SiGe homojunction diodes is shown in Fig. 1(a). Initially, SiGe layers are epitaxially grown by rapid thermal chemical vapor deposition (RTCVD). Before loading into the reactor, the heavily doped n -type Si (001) substrates of $\rho \sim 0.003 \Omega \text{ cm}$ are cleaned by $\text{H}_2\text{SO}_4:\text{H}_2\text{O}_2$ (2.5:1) for 15 min followed by diluted HF (1:50) for 1 min. Those wafers are then heated to 950°C in a hydrogen (H_2) carrier for 5 min to remove the residual oxide before the epitaxial growth started. Dichlorosilane (SiH_2Cl_2) and diluted germane (GeH_4) in H_2 (0.8%) are the precursors for SiGe growth. Diluted phosphine (PH_3) and diborane (B_2H_6) in H_2 (100 ppm) are used for the *in situ* doping. After high-temperature baking, an n^+ -SiGe layer is grown followed by the deposition of p^+ -SiGe layer by fast switching of the dopant gases. The diodes of Ge fractions of 0.14, 0.21, and 0.27 are grown at 625°C with the total thicknesses of 50, 66, and 40 nm, and the diode of Ge fraction of 0.35 is grown at 575°C with a thickness of 30 nm. The thicknesses of p^+ and n^+ layers for each Ge fraction are given in Table I. The layer thicknesses, Ge fraction, and doping concentrations are determined by secondary ion mass spectrometry (SIMS) [for example, see Fig. 1(b) for a $\text{Si}_{0.79}\text{Ge}_{0.21}$ tunneling diode]. The expected critical thicknesses of the metastable SiGe films on Si for those four diodes of Ge fractions of 0.14, 0.21, 0.27, and 0.35 are 450, 180, 80, and

Manuscript received March 9, 2013; revised May 8, 2013 and June 3, 2013; accepted June 4, 2013. Date of publication June 26, 2013; date of current version July 19, 2013. This work was supported by DARPA under Grant AFRL FA8650-08-C-7806. The review of this paper was arranged by Editor G. Niu.

The authors are with the Department of Electrical Engineering and the Princeton Institute for the Science and Technology of Materials, Princeton University, NJ 08544 USA (e-mail: jiunyun@princeton.edu; sturm@princeton.edu).

Digital Object Identifier 10.1109/TEDE.2013.2267172

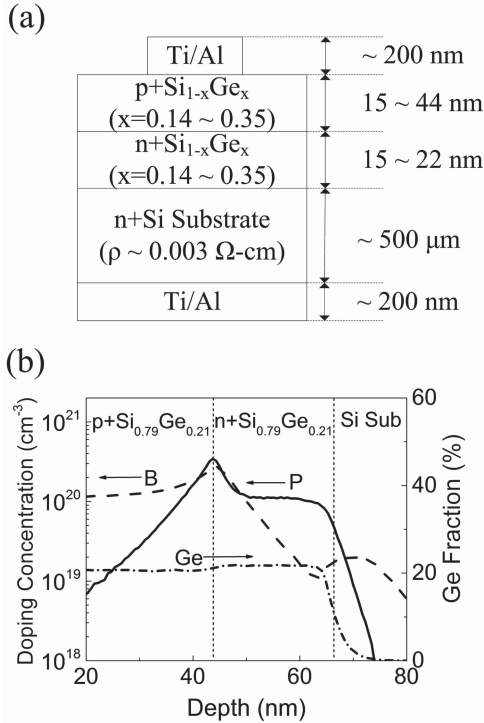


Fig. 1. (a) Device structure of SiGe tunneling diodes and (b) Ge, B, and P concentrations in a $\text{Si}_{0.79}\text{Ge}_{0.21}$ tunneling diode measured by SIMS.

TABLE I
LAYER THICKNESS OF $\text{P}^+\text{-SiGe}/\text{N}^+\text{-SiGe}$ DIODES

Ge Fraction (%)	Thickness of $\text{p}^+\text{-SiGe}$ Layer (nm)	Thickness of $\text{n}^+\text{-SiGe}$ Layer (nm)
14	33	17
21	44	22
27	24	17
35	15	15

35 nm, respectively [10]. Thus, we expect that those films are biaxially compressively strained, pseudomorphic to the Si substrates. Finally, square mesas are dry-etched with an area of $25 \times 25 \mu\text{m}^2$. The Ti/Al is deposited on top of the mesas and bottom of the wafers as ohmic contacts for electrical measurement.

III. FORWARD-BIASED BAND-TO-BAND TUNNELING

A. Kane's Model on Tunneling

In a tunneling diode, both n -type and p -type bulk regions are degenerately doped, so the Fermi level is pushed into the conduction (valence) band in the n -type (p -type) region. Therefore, at small forward biases, electrons in the conduction band in the n -type region can tunnel through the barrier to the valence band in the p -type region. As the bias increases, lowering the band on the p -type side, more empty states in the p -type valence band are provided at the same energy levels of electrons in the n -type conduction band, leading to increased tunneling current. When the voltage is raised further, the valence-band edge at p -type side falls below the conduction-band edge at n -type side, so electron tunneling from the n -type conduction band to the p -type valence band is no

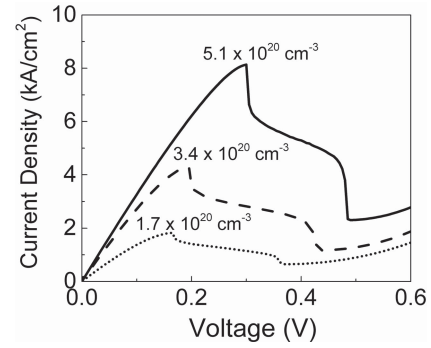


Fig. 2. Room-temperature J - V curves of $\text{p}^+\text{-n}^+\text{-Si}_{0.73}\text{Ge}_{0.27}$ tunnel diodes with three different boron concentrations at a fixed phosphorus level of $1.0 \times 10^{20} \text{ cm}^{-3}$.

longer possible. Thus, there exists a voltage range where the tunneling current decreases, leading to NDR. The NDR feature in forward bias is widely used as a confirmation of the BTBT. The tunneling probability strongly depends on the bandgap energy and the electric field. A classical model of the BTBT in forward bias was proposed in [11]. The analytical expression of the peak tunneling-current density at forward bias is presented in [12] as follows:

$$J_{\text{peak,FB}} = \frac{em^*}{2\pi^2\hbar^3} \exp(-\pi\sqrt{m^*E_g^3}/2\sqrt{2e\hbar E_{\text{field}}}) \cdot \frac{E_{\perp}}{2} \cdot D \quad (1)$$

$$E_{\perp} = \frac{4\sqrt{2e\hbar}|E_{\text{field}}|}{3\pi\sqrt{m^*E_g}} \quad (2)$$

$$D \equiv \int [f_c(E) - f_v(E)] \cdot \left[1 - e^{-\frac{2E_x}{E_{\perp}}}\right] dE \quad (3)$$

where m^* is the effective mass of electrons in semiconductors, E_g is the bandgap energy, E_{field} is the electric field in the p - n junction, E_{\perp} is a measure of the range of transverse momentum, D is the effective density of states, $f_c(E)$ and $f_v(E)$ are the Fermi-Dirac distribution functions of electrons in the conduction band of n -type bulk region and in the valence band of p -type bulk region, and E_s is the smaller of E_n and E_p , that are the electron or hole energy measured from the edges of the conduction band or the valence band. In practice, D is evaluated using the expressions derived in [11]. Following Fair's work on Si Zener tunneling [13], we use $m^* = 0.33 m_0$, where m_0 is the free electron mass, throughout this paper for the calculation of BTBT current density.

B. Experimental Results

Experimentally, we first study the effect of electric field on BTBT by changing boron concentration (N_A : 1.7 – $5.1 \times 10^{20} \text{ cm}^{-3}$) with a fixed phosphorus level of $N_D \sim 1.0 \times 10^{20} \text{ cm}^{-3}$ in $\text{Si}_{0.73}\text{Ge}_{0.27}$ tunneling diodes. NDR is clearly seen for all diodes (Fig. 2), a confirmation of BTBT and the high material quality for those devices [14]. As the boron concentration increases, the peak current in forward bias, $J_{\text{peak,FB}}$, increases due to a higher electric field and a reduced tunneling barrier. The peak voltage is shifted to a larger value because of the series resistance. The series resistance of those devices is dominated by the spreading resistance in the Si

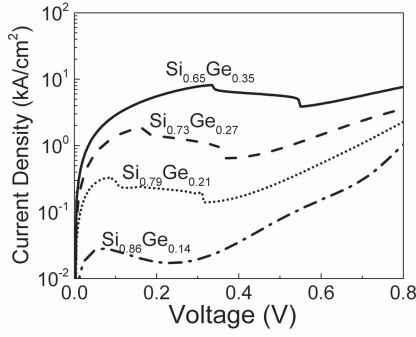


Fig. 3. Room-temperature J - V curves of $p^+-n^+-\text{Si}_{1-x}\text{Ge}_x$ tunnel diodes ($x = 0.14, 0.21, 0.27,$ and 0.35).

substrate. Thus, the shift of peak voltage would depend only on the peak current (density), which increases with the boron level. A $J_{\text{peak,FB}}$ of 8.2 kA/cm^2 is achieved, which we believe to be the highest reported for all Si-based tunneling diodes grown by CVD.

Next, to study the effect of Ge fraction, strained SiGe tunneling diodes of four different Ge fractions are grown and fabricated. The I - V curves are shown in Fig. 3 with NDR clearly observed for each diode. As the Ge fraction increases from 0.14 to 0.35, $J_{\text{peak,FB}}$ increases from 0.03 to 8.2 kA/cm^2 , because of the reduced bandgap energy. The shift of the peak voltage with Ge fraction is also attributed to the presence of series resistance.

To understand how the forward-biased BTBT current is affected by SiGe bandgap energy, we use the empirical model of bandgap in [15] based on their photoluminescence measurements at 4 K, with a subtraction of 50 meV for the difference between their measurements at 4 K and ours at room temperature [16], to convert the measured Ge fractions to bandgap energies as follows:

$$E_g(300 \text{ K}) = 1.17 - 0.896x + 0.396x^2 - 0.05 \text{ eV} \quad (4)$$

where x is the germanium fraction in $\text{Si}_{1-x}\text{Ge}_x$ alloys. The Ge dependence of forward-biased BTBT current is investigated by plotting $J_{\text{peak,FB}}$ versus Ge fraction in Fig. 4(a). Using the doping profiles measured by SIMS and assuming full activation of all dopants in SiGe by low-temperature CVD [17], the associated electric field can be estimated by a device simulator. The theoretical current density is calculated using (1)–(4) and is compared with the experimental results. Good agreement in peak current density between model predictions and experimental data is demonstrated over three orders of magnitude up to the level of 10 kA/cm^2 .

To isolate the effect of Ge fraction, the effect of different doping profiles in samples at different Ge fractions must be removed (e.g., N_A is varied from 1.2 to $3.6 \times 10^{20} \text{ cm}^{-3}$ and N_D is varied from 0.7 to $2.5 \times 10^{20} \text{ cm}^{-3}$). To do this (Fig. 5), we use (1)–(3) to predict how the peak tunneling-current density scales with the peak electric field and then adjust the data points to reflect a single dopant profile at different Ge fractions. First, we calculate the peak voltage (V_{peak}) and its electric field (E_{field}) by assuming perfectly abrupt doping profiles [12] and no series resistance with a single set of fixed doping levels of $N_A = 1.2 \times 10^{20} \text{ cm}^{-3}$

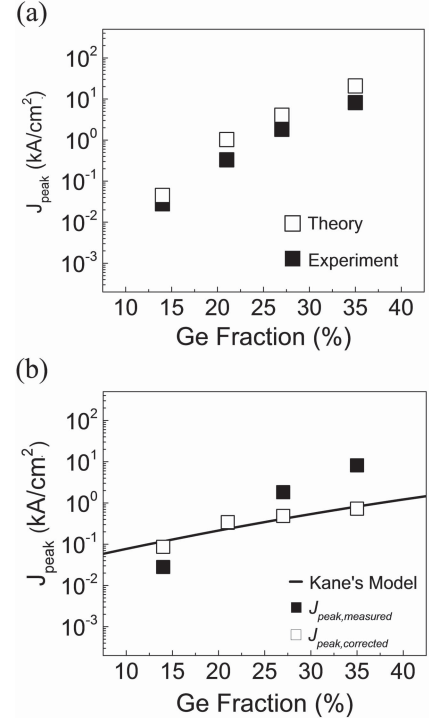


Fig. 4. (a) $J_{\text{peak,FB}}$ versus Ge fraction. Solid and open squares are the experimental results and model predictions, respectively. The model predictions include the actual doping profiles in each device. (b) $J_{\text{peak,FB}}$ versus Ge fraction with a doping correction procedure in Fig. 5 to remove the doping effects. Solid squares: the experimental data. Open squares: data corrected to a single set of fixed doping levels of $N_A = 1.2 \times 10^{20} \text{ cm}^{-3}$ and $N_D = 0.7 \times 10^{20} \text{ cm}^{-3}$. Solid line: theoretical calculation using (1)–(4).

and $N_D = 0.7 \times 10^{20} \text{ cm}^{-3}$ for each Ge fraction. Then we calculate the peak current density ($J_{\text{peak,abrupt}}$) using (1)–(3). Next, we use the actual doping profiles measured by SIMS to calculate V_{peak} and E_{field} using a device simulator. Then, we calculate the peak current density ($J_{\text{peak,SIMS}}$) using (1)–(3) at that field. The ratio of these two current densities gives a correction factor to be applied to the experimental data for the adjustment of the doping levels for all Ge fractions, so a comparison of data with a single set of doping profiles ($N_A = 1.2 \times 10^{20} \text{ cm}^{-3}$ and $N_D = 0.7 \times 10^{20} \text{ cm}^{-3}$) can be made. Then, we measure the I - V curves of the devices to obtain $J_{\text{peak,measured}}$ and calculate the corrected peak current density ($J_{\text{peak,corrected}}$) by the relationship as follows:

$$J_{\text{peak,corrected}} = J_{\text{peak,measured}} \cdot \frac{J_{\text{peak,abrupt}}}{J_{\text{peak,SIMS}}} \quad (5)$$

The experimental ($J_{\text{peak,measured}}$) and corrected peak current density ($J_{\text{peak,corrected}}$) as a function of Ge fraction (solid and open squares) and also a theoretical prediction for a single set of doping levels (solid line) are shown in Fig. 4(b). For Ge fraction of 0.14, $J_{\text{peak,corrected}}$ is larger than $J_{\text{peak,measured}}$ because the actual doping profiles are not abrupt, resulting in a smaller electric field and thus a larger tunneling barrier. For higher Ge fractions, instead, $J_{\text{peak,measured}}$ are larger than $J_{\text{peak,corrected}}$ because of the higher doping levels for those diodes. No adjustable parameters are used in the correction process. Significantly, there is good agreement between the slope of the theoretical calculation of peak tunneling current

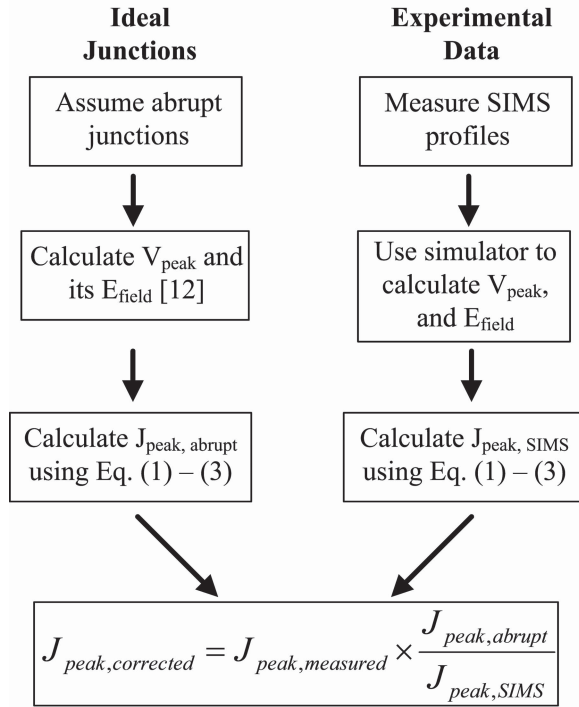


Fig. 5. Correction procedure of peak current density (J_{peak}) for each Ge fraction to a single set of fixed doping levels.

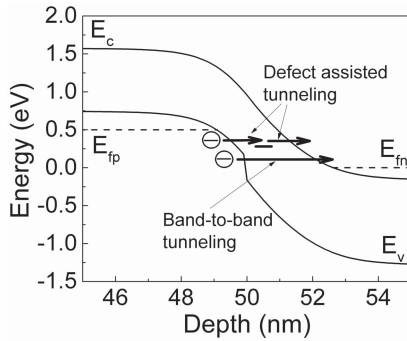


Fig. 6. Schematic of band energy diagram of $p^+-\text{Si}_{0.73}\text{Ge}_{0.27}/n^+-\text{Si}$ to show the processes of band-to-band tunneling and defect-assisted tunneling in reverse bias.

versus bandgap and data corrected to a single set of doping levels. This confirms that Kane's model can be used to predict the BTBT of $p^+-\text{SiGe}/n^+-\text{SiGe}$ homojunctions at current density up to the level of 10 kA/cm^2 in forward bias.

IV. REVERSE-BIASED BAND-TO-BAND TUNNELING

A. Importance of NDR

The operation of TFETs relies on BTBT under reverse bias, also known as Zener tunneling [18], [19]. Unlike NDR in forward bias, there is no simple and clear feature in reverse bias that can be used to confirm that the observed current is due to BTBT. For example, defect states in the bandgap at the junction can lead to DAT [9], in which an electron first tunnels from the valence band of p -type region to a defect state in the bandgap of depletion region and then tunnels from the defect state to the conduction band of n -type region (Fig. 6). Because each step of this process has a much lower tunneling barrier

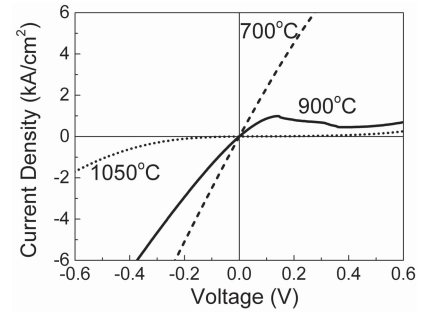


Fig. 7. Room-temperature J - V curves of $p^+-\text{Si}_{0.73}\text{Ge}_{0.27}/n^+-\text{Si}$ heterojunction tunneling diodes with three different annealing temperatures.

than the direct BTBT, the two-step DAT process can easily swamp the BTBT. To probe the effect of the DAT process, we examine tunneling in both forward and reverse biases in $p^+-\text{SiGe}/n^+-\text{Si}$ heterojunction tunneling diodes. They are not fabricated by the *in situ* CVD doping technique, but by first doping the Si substrates by ion implantation of phosphorus. The implant doses of 5×10^{14} , 7×10^{14} , 1×10^{15} , and $2 \times 10^{15} \text{ cm}^{-2}$ at energies of 15, 40, 80, and 120 keV, respectively, are used to achieve a phosphorus concentration $\sim 2 \times 10^{20} \text{ cm}^{-3}$. The wafers are then annealed in the RTCVD reactor (700–1050 °C) followed by the SiGe epitaxy with the *in situ* boron doping. The boron level is $2 \times 10^{20} \text{ cm}^{-3}$. A mesa process similar to that for the homojunction diodes (in Section II) is used to fabricate the heterojunction devices.

For a relatively low annealing temperature (700 °C), a fairly high current with ohmic characteristics is observed at both forward and reverse biases, with no hint of NDR (Fig. 7). At 900 °C annealing, a lower peak current with NDR at forward bias is observed with a lower current in reverse bias as well. We hypothesize that for the sample of 700 °C annealing, the tunneling current in forward and reverse biases is dominated by the DAT process because of the incomplete annealing of the implanted damage, which swamped the true BTBT current. The defect density (and thus the DAT process) is reduced by 900 °C annealing so that NDR at forward bias and the true BTBT current density could be observed. In the sample annealed at 1050 °C, there is no NDR and current densities at forward and reverse biases are much lower, probably because the diffusion of dopants at 1050 °C reduces the junction abruptness and the electric field. The main message is that if NDR is not observed (e.g., at 700 °C), the observed current in both forward and reverse biases has a large DAT component, and it cannot be used as a true measure of the BTBT current. Thus, we strongly suggest that to use reverse-biased tunneling data to calibrate the BTBT model, a demonstration of NDR at forward bias is necessary to exclude the contribution of DAT current.

B. Effect of Series Resistance

Zener tunneling (reverse-biased BTBT) is usually characterized at moderate doping levels ($\sim 10^{18} \text{ cm}^{-3}$). At such doping levels, the current density is very low ($\sim 10^{-4} \text{ kA/cm}^2$ [12]), so the effect of series resistance can be ignored. For SiGe TFETs, the operation at electric field $> 10^7 \text{ V/m}$ is desired,

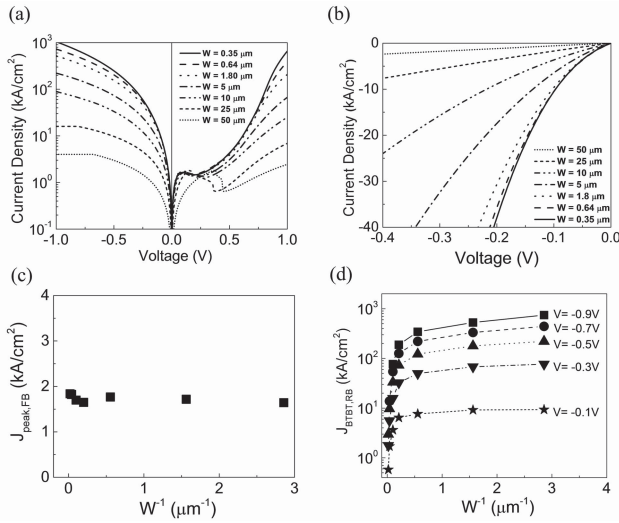


Fig. 8. (a) Room-temperature J - V curves of $\text{Si}_{0.73}\text{Ge}_{0.27}$ homojunction tunneling diodes with different mesa widths, (b) enlarged view of J - V curves at small reverse biases of (a), (c) $J_{\text{peak,FB}}$ versus inverse of mesa width (W^{-1}), and (d) reverse-biased BTBT current density ($J_{\text{BTBT,FB}}$) versus (W^{-1}) at $V = -0.1, -0.3, -0.5, -0.7,$ and -0.9 V.

resulting in a high current level. Thus, the effect of series resistance such as current crowding must be considered for a precise calibration of the BTBT in SiGe tunneling diodes. Guo *et al.* suggested that by scaling down the mesa width (W) of the diodes the current crowding can be eliminated [20]. Therefore, we fabricated several $\text{Si}_{0.73}\text{Ge}_{0.27}$ homojunction diodes with mesa widths of 50–0.35 μm by a combination of photolithography and electron-beam lithography. The wafers are the same as those used for the forward-biased BTBT study in Section III. The current density at forward bias is shown in Fig. 8(a) with clear NDR for each mesa width. Peak current density versus the inverse of mesa width (W^{-1}) is also shown in Fig. 8(c). The average of $J_{\text{peak,FB}}$ is 1.73 kA/cm^2 and the deviations are within $\pm 5\%$, which shows the negligible contribution of the leakage current via the mesa edges [21]. In reverse bias, the current density approaches constant levels as the mesa width decreases [Fig. 8(b) and (d)]. Because NDR is clearly seen at forward bias and the effect of series resistance is eliminated by scaling down the mesa width, we believe that the plateaus of the current density that are shown in Fig. 8(d) are the true BTBT current densities in reverse bias.

C. Comparison of Experimental Data and Model

We now seek to present the BTBT in reverse bias as a function of Ge fraction and electric field for device designers to model the TFETs and related devices. Similar to the peak current density at forward bias, the reverse-biased BTBT current ($J_{\text{BTBT,FB}}$) also strongly depends on the electric field and bandgap energy. An analytical form of $J_{\text{BTBT,FB}}$ in reverse bias based on Kane's model was presented in [13] as follows:

$$J_{\text{BTBT,FB}} = \frac{\sqrt{2m^*}e^3 E_{\text{field}} V}{4\pi^3 \hbar^2 \sqrt{E_g}} \cdot \exp\left(\frac{-4\sqrt{2m^*}E_g^3}{3e\hbar E_{\text{field}}}\right) \quad (6)$$

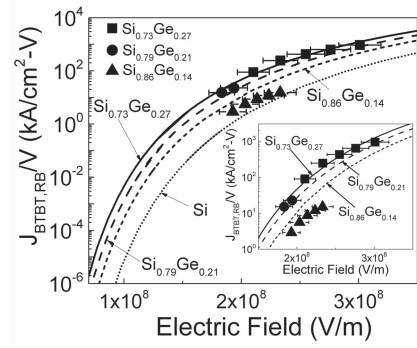


Fig. 9. $J_{\text{BTBT,FB}}/V$ in reverse bias versus electric field for SiGe BTBT. Symbols are the experimental data and multiple lines are the theoretical predictions based on (4) and (6). Inset: an enlarged view at high electric fields ($2\text{--}3 \times 10^8$ V/m).

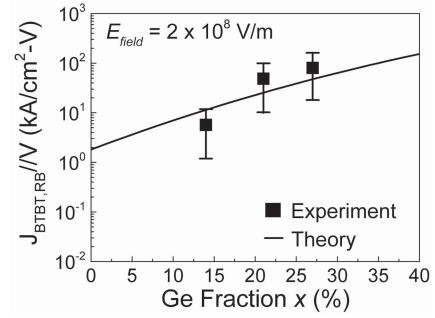


Fig. 10. $J_{\text{BTBT,FB}}/V$ at reverse bias versus Ge fraction at $E_{\text{field}} \sim 2 \times 10^8$ V/m. Squares are the experimental data, error bars are the resulting variations of $J_{\text{BTBT,FB}}$ by the horizontal error bars in the electric field (Fig. 9), and the solid line is the model prediction.

where V is the applied voltage. The electron tunneling probability depends on the tunneling distance. In a semiconductor p-n junction, the tunneling distance is inversely proportional to the peak electric field [11], so $\log(J_{\text{BTBT,FB}})$ in (6) depends on the inverse of the electric field. The parameter of $J_{\text{BTBT,FB}}/V$ is plotted versus electric field (E_{field}) for different Ge fractions in Fig. 9, along with theoretical calculations based on (6). As in forward bias, the measured SIMS doping profiles and the device simulator are used to calculate the peak electric field for all devices. The horizontal error bars in electric field, which result from a deviation of $\pm 15\%$ in the doping levels, are also presented.

At small electric fields ($< 1 \times 10^8$ V/m), (6) predicts that $J_{\text{BTBT,FB}}/V$ arises sharply with E_{field} . On the other hand, as the electric field increases further, $J_{\text{BTBT,FB}}/V$ increases much more slowly. For example, at low fields ($E_{\text{field}} = 5 \times 10^7$ V/m), $J_{\text{BTBT,FB}}/V$ of $\text{Si}_{0.73}\text{Ge}_{0.27}$ (Fig. 9, solid line) increases by a factor of 2×10^5 as E_{field} increases by 60%. At $E_{\text{field}} = 2 \times 10^8$ V/m, however, it only increases by a factor of 30. Our data of reverse-biased tunneling-current density at $E_{\text{field}} > 2 \times 10^8$ V/m, which is between 3 and 1000 kA/cm^2 V, are in close agreement with the model predictions (see the inset in Fig. 9). This is fortuitous as our data points of $J_{\text{BTBT,FB}}/V$ are three to five orders of magnitude higher than those for Si BTBT at low electric fields ($< 1 \times 10^8$ V/m) [13], [22], where (6) is conventionally applied.

To isolate the effect of bandgap energy, $J_{BTBT, RB}/V$ versus Ge fraction at $E_{\text{field}} = 2 \times 10^8$ is shown in Fig. 10 by extrapolating between the points in Fig. 9 along with the model of (4) and (6). The $\pm 6\%$ uncertainty in the peak electric field is used to estimate the error in BTBT current. Within an uncertainty in current that is introduced by the uncertainty in electric field, the results show that (4) and (6) can be used to model the dependence of $J_{BTBT, RB}$ on the Ge fraction. More complete modeling might include the effect of heavy doping on bandgap energy, and the effect of strains on the effective density of states and the effective mass of electrons in SiGe alloys, which are not considered in this paper.

V. CONCLUSION

A quantitative study of the BTBT in forward and reverse biases in $p^+-\text{SiGe}/n^+-\text{SiGe}$ homojunctions was presented. We observed a high peak tunneling-current density of 8.2 kA/cm^2 in a $\text{Si}_{0.65}\text{Ge}_{0.35}$ diode, which we believed to be the highest among all Si-based tunneling diodes grown by CVD. Through eliminating series resistance, a reverse-biased BTBT tunneling current density in a $\text{Si}_{0.73}\text{Ge}_{0.27}$ tunneling diode up to $\sim 1000 \text{ kA/cm}^2$ at -1 V was achieved. The observation of NDR in forward bias was crucial for establishing that the true BTBT current dominates the current in the reverse bias and not the DAT current. A comparison of experimental data with Kane's model was presented, which showed a close match in both forward and reverse biases. This experimental verification of the models enables device designers to predict the dependence of the tunneling current on germanium fraction and can be used in device simulators to predict the performance of TFETs and other relevant devices.

ACKNOWLEDGMENT

The authors thank S. Koester (now at the University of Minnesota), I. Lauer, A. Majumdar, and P. Solomon at IBM T. J. Watson Research Center, Yorktown Heights, NY for stimulating discussions and providing some of the implanted substrates that were used in the SiGe/Si heterojunction work.

REFERENCES

- [1] A. M. Ionescu and H. Riel, "Tunnel field-effect transistors as energy-efficient electronic switches," *Nature*, vol. 479, pp. 329–337, Nov. 2011.
- [2] W. Y. Choi, B.-G. Park, J. D. Lee, and T.-J. K. Liu, "Tunneling field-effect transistors (TFETs) with subthreshold swing (SS) less than 60 mV/dec ," *IEEE Electron Device Lett.*, vol. 28, no. 8, pp. 743–745, Aug. 2007.
- [3] M. Schmidt, R. A. Minamisawa, S. Richter, A. Schäfer, D. Buca, J. M. Hartmann, Q. T. Zhao, and S. Mantl, "Unipolar behavior of asymmetrically doped strained $\text{Si}_{0.5}\text{Ge}_{0.5}$ tunneling field-effect transistors," *Appl. Phys. Lett.*, vol. 101, pp. 123501-1–123501-4, Sep. 2012.
- [4] K. K. Bhuiwarka, J. Schultz, and I. Eisele, "Scaling the vertical tunnel FET with tunnel bandgap modulation and gate workfunction engineering," *IEEE Trans. Electron Devices*, vol. 52, no. 5, pp. 909–917, May 2005.
- [5] L.-E. Wernersson, S. Kabeer, V. Zela, E. Lind, J. Zhang, W. Seifert, T. H. Kosel, and A. Seabaugh, "A combined chemical vapor deposition and rapid thermal diffusion process for SiGe Esaki diodes by ultrashallow junction formation," *IEEE Trans. Nanotechnol.*, vol. 4, no. 5, pp. 594–598, Sep. 2005.
- [6] J. Y. Li, J. C. Sturm, A. Majumdar, I. Lauer, and S. Koester, "Bandgap dependence of band-to-band tunneling and defect-mediated excess currents in SiGe/Si heterojunction tunnel diodes grown by RTCVD," in *Proc. 67th Ann. Device Res. Conf.*, Jun. 2009, pp. 99–100.

- [7] O. M. Nayfeh, C. N. Chlérigh, J. L. Hoyt, and D. A. Antoniadis, "Measurement of enhanced gate-controlled band-to-band tunneling in highly strained silicon-germanium diodes," *IEEE Electron Device Lett.*, vol. 29, no. 5, pp. 468–470, May 2008.
- [8] L. Esaki, "New phenomenon in narrow germanium p-n junctions," *Phys. Rev.*, vol. 109, no. 2, pp. 603–604, Jan. 1958.
- [9] A. G. Chynoweth, W. L. Feldmann, and R. A. Logan, "Excess tunnel current in silicon Esaki junctions," *Phys. Rev.*, vol. 121, no. 3, pp. 684–694, Feb. 1961.
- [10] R. People and J. C. Bean, "Calculation of critical layer thickness versus lattice mismatch for $\text{Ge}_x\text{Si}_{1-x}/\text{Si}$ strained-layer heterostructures," *Appl. Phys. Lett.*, vol. 47, no. 3, pp. 322–324, Aug. 1985.
- [11] E. O. Kane, "Theory of tunneling," *J. Appl. Phys.*, vol. 32, no. 1, pp. 83–91, Jan. 1961.
- [12] S. M. Sze and K. K. Ng, *Physics of Semiconductor Devices*. New York, NY, USA: Wiley, 2006, ch. 8.
- [13] R. B. Fair and H. W. Wivell, "Zener and avalanche breakdown in As-implanted low-voltage Si n-p junctions," *IEEE Trans. Electron Devices*, vol. 23, no. 5, pp. 512–518, May 1976.
- [14] B. D. Weaver, P. E. Thompson, N. Jin, S.-Y. Chung, A. T. Rice, and P. R. Berger, "Radiation tolerance of $\text{Si}/\text{Si}_{0.6}\text{Ge}_{0.4}$ resonant interband tunneling diodes," *J. App. Phys.*, vol. 95, no. 11, pp. 6406–6408, Jun. 2004.
- [15] D. J. Robbins, L. T. Canham, S. J. Barnett, A. D. Pitt, and P. Calcott, "Near-band-gap photoluminescence from pseudomorphic $\text{Si}_{1-x}\text{Ge}_x$ single layers on silicon," *J. Appl. Phys.*, vol. 71, no. 3, pp. 1407–1414, Feb. 1992.
- [16] R. Braunstein, A. R. Moore, and F. Herman, "Intrinsic optical absorption in germanium-silicon alloys," *Phys. Rev.*, vol. 109, no. 3, pp. 695–710, Feb. 1958.
- [17] J. Noh, S. Takehiro, M. Sakuraba, and J. Murota, "Relationship between impurity (B or P) and carrier concentration in SiGe(C) epitaxial film produced by thermal treatment," *Appl. Surf. Sci.*, vol. 224, pp. 77–81, Mar. 2004.
- [18] A. G. Chynoweth, W. L. Feldmann, R. A. Logan, and G. L. Pearson, "Internal field emission at narrow silicon and germanium p-n junctions," *Phys. Rev.*, vol. 118, no. 2, pp. 425–434, Apr. 1960.
- [19] G. A. M. Hurkx, "On the modeling of tunneling currents in reverse-biased p-n junctions," *Solid-State Electron.*, vol. 32, no. 8, pp. 665–668, 1989.
- [20] X. Guo and E. F. Schubert, "Current crowding and optical saturation effects in GaInN/GaN light-emitting diodes grown on insulating substrates," *Appl. Phys. Lett.*, vol. 78, no. 21, pp. 3337–3339, May 2001.
- [21] P. Fay, J. Lu, Y. Xu, G. H. Bernstein, D. H. Chow, and J. N. Schulman, "Microwave performance and modeling of InAs/AlSb/GaSb resonant interband tunneling diodes," *IEEE Trans. Electron Devices*, vol. 49, no. 1, pp. 19–24, Jan. 2002.
- [22] J. M. C. Stork and R. D. Isaac, "Tunneling in base-emitter junctions," *IEEE Trans. Electron Devices*, vol. 30, no. 11, pp. 1527–1534, Nov. 1983.



Jiun-Yun Li (S'06) received the M.S. degree in electrical and computer engineering from the University of Maryland, College Park, MD, USA, in 2007. He is currently pursuing the Ph.D. degree in electrical engineering with Princeton University, Princeton, NJ, USA.



James C. Sturm (S'81–M'85–SM'95–F'01) received the Ph.D. degree from Stanford University, Stanford, CA, USA, in 1985.

He is currently the Macaleer Professor of engineering and applied science with Princeton University Princeton, NJ, USA.